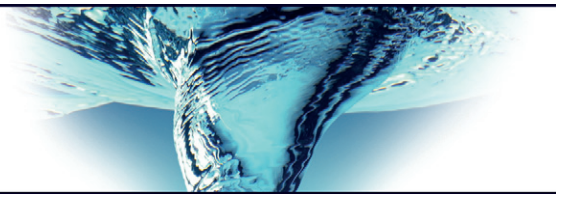
J. Fluid Mech. (2018), *vol.* 846, R2, doi:10.1017/jfm.2018.327



JFM RAPIDS
journals.cambridge.org/rapids

Phase-response analysis of synchronization for periodic flows

Kunihiko Taira[1,†] **and Hiroya Nakao**[2]

[1]Department of Mechanical Engineering, Florida State University, Tallahassee, FL 32310, USA

[2]Department of Systems and Control Engineering, Tokyo Institute of Technology, Tokyo 152-8552, Japan

(Received 29 January 2018; revised 4 April 2018; accepted 13 April 2018; first published online 3 May 2018)

We apply phase-reduction analysis to examine synchronization properties of periodic fluid flows. The dynamics of unsteady flows is described in terms of the phase dynamics, reducing the high-dimensional fluid flow to its single scalar phase variable. We characterize the phase response to impulse perturbations, which can in turn quantify the influence of periodic perturbations on the unsteady flow. These insights from phase-based analysis uncover the condition for synchronization. In the present work, we study as an example the influence of periodic external forcing on an unsteady cylinder wake. The condition for synchronization is identified and agrees closely with results from direct numerical simulations. Moreover, the analysis reveals the optimal forcing direction for synchronization. Phase-response analysis holds potential to uncover lock-on characteristics for a range of periodic flows.

Key words: low-dimensional models, nonlinear dynamical systems, wakes

1. Introduction

Synchronization is a phenomenon where a system with oscillatory dynamics exhibits its oscillations in unison (Winfree 1967; Guckenheimer 1975; Kuramoto 1984; Strogatz 2000; Pikovsky, Rosenblum & Kurths 2001). This phenomenon was first reported by Huygens, the inventor of the pendulum clock, who noticed that the pendulums of two different clocks on a beam always swing in phase or antiphase (Pikovsky *et al.* 2001). Since then, there have been a variety of studies on uncovering the synchronization mechanisms of oscillators, including oscillatory chemical reactions (Kuramoto 1984), synchronous flashing of fireflies (Buck 1988) and jet lag through inter-neuronal communications (Yamaguchi *et al.* 2013).

Even if the overall physics involving synchronization is complex and high-dimensional, the analysis of synchronization can be simplified immensely for weak

† Email address for correspondence: ktaira@fsu.edu

© Cambridge University Press 2018

https://doi.org/10.1017/jfm.2018.327 Published online by Cambridge University Press

perturbations by considering its phase dynamics. Such a formulation allows us to focus solely on the scalar phase of the oscillator instead of having to be concerned with the full state dynamics. This approach is known as phase-reduction analysis and enables an elegant formulation to examine a set of interacting oscillators (Winfree 1967; Kuramoto 1984; Ermentrout & Terman 2010; Nakao 2016). Phase-based analysis reveals its strength in analysing networked dynamics and the emergence of synchronized motion and patterns.

While phase-reduction analysis has been applied to numerous problems in biological (Winfree 1967; Ermentrout & Terman 2010) and chemical systems (Kuramoto 1984), there has been limited use in the field of unsteady fluid dynamics, especially with regard to synchronization. Some of the few applications of phase-based analysis to fluid mechanics have been concerned with Hele-Shaw flows (Kawamura & Nakao 2013, 2015). In the present work, we apply phase-based analysis to full nonlinear periodic wake flows to examine synchronization. The discussion herein provides an alternative perspective on examining fluid flows through a single scalar phase variable, which enables significant simplification to the theoretical analysis and reduction in computational and experimental efforts to examine lock on.

In what follows, we present the phase-reduction analysis (Nakao 2016) in the context of periodic fluid flows. The perspective to examine fluid flows with phase dynamics is provided in § 2, with focus on analysing synchronization of fluid flows to external excitation. The phase-reduction analysis is then applied to an example of an unsteady cylinder wake with periodic forcing in § 3. The condition for synchronization is determined from phase-response analysis, revealing the Arnold tongue for lock on. Concluding remarks are offered in § 4. The approach described below can be performed through simulations and experiments, making it attractive for the analysis of a range of fluid flow problems, including unsteady flows, active flow control, fluid–structure interactions and reacting flows.

2. Phase-reduction analysis

2.1. *Phase-reduction analysis of periodic flows*

Let us consider the dynamics of incompressible flow, represented as

$$\dot{\boldsymbol{q}} = \boldsymbol{F}(\boldsymbol{q}), \tag{2.1}$$

where $\boldsymbol{q}$ is the flow variable which has a stable periodic flow (limit cycle) $\boldsymbol{q}_0$ satisfying

$$\boldsymbol{q}_0(\boldsymbol{x}, t+T) = \boldsymbol{q}_0(\boldsymbol{x}, t). \tag{2.2}$$

For this limit cycle, the periodicity is denoted by T which gives the natural frequency of $\omega_n = 2\pi/T$. As expressed in (2.2), flows are generally described in terms of spatial and temporal variables. For incompressible flow, we can take $\boldsymbol{q}$ to be the velocity vector. In this work, we instead describe the state of the oscillatory flow using the phase θ of the limit cycle, such that

$$\dot{\theta}(t) = \omega_n, \quad \text{where } \theta(t) \in [-\pi, \pi]. \tag{2.3}$$

The main idea here is to reduce the description of the flow from the flow state $\boldsymbol{q}(\boldsymbol{x}, t)$ to a single scalar phase variable θ (Winfree 1967; Guckenheimer 1975; Kuramoto 1984). If we have a periodic flow, the phase can point back to the full periodic flow field $\boldsymbol{q}_0(\theta)$. The description of the phase is given in figure 1 for an example of

https://doi.org/10.1017/jfm.2018.327 Published online by Cambridge University Press

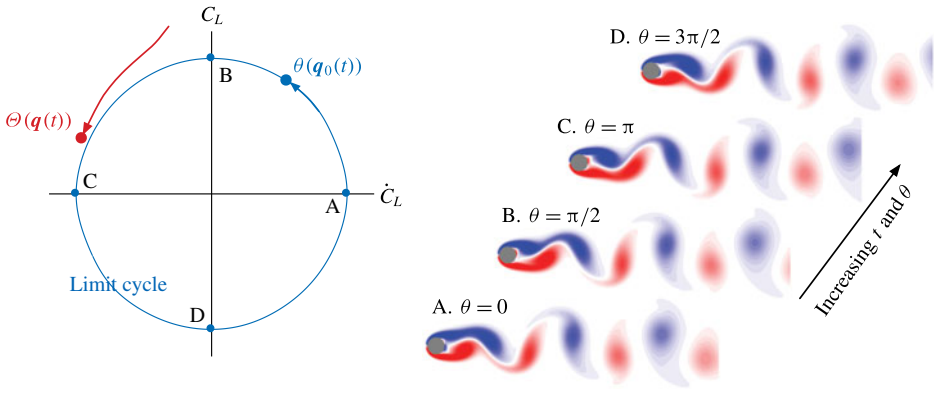


FIGURE 1. Definition of phase θ and phase function Θ with C_L and $\dot{C}_L$ for cylinder flow at a Reynolds number of $Re = 100$. Vorticity fields are shown at representative phases.

periodic cylinder flow, which will be examined in detail later in § 3. In this example, the phase dynamics of the flow can be understood by examining the lift C_L on the cylinder, which holds the same synchronization properties as the flow. The limit cycle of periodic cylinder flow is shown in blue over the $\dot{C}_L$–C_L phase space, with the vorticity fields visualized at representative phases.

The above characterization of the phase is limited to flow states that reside on the limited cycle $\boldsymbol{q}_0$. We can extend the concept of phase in the basin of the limit cycle and define a phase function $\Theta(\boldsymbol{q}(\boldsymbol{x}, t))$ that returns the phase, i.e. $\theta = \Theta(\boldsymbol{q})$. The phase function can capture the phase dynamics off the limit cycle, as illustrated in red in figure 1. By combining (2.1) and (2.3), we observe that the phase function satisfies

$$\dot{\theta}(t) = \dot{\Theta}(\boldsymbol{q}) = \nabla_{\boldsymbol{q}}\Theta(\boldsymbol{q}) \cdot \dot{\boldsymbol{q}} = \nabla_{\boldsymbol{q}}\Theta(\boldsymbol{q}) \cdot \boldsymbol{F}(\boldsymbol{q}) = \omega_n. \tag{2.4}$$

This phase function enables the phase to be defined over the entire phase space. A surface of constant phase is referred to as an isochron and is directed perpendicular to $\nabla\Theta(\boldsymbol{q})$ (Guckenheimer 1975). The notion of isochron is closely related to the eigenfunction of the Koopman operator (Mauroy & Mezić 2012).

2.2. *Phase-reduction analysis of perturbed flows*

Now, let us consider perturbing the governing dynamics by

$$\dot{\boldsymbol{q}} = \boldsymbol{F}(\boldsymbol{q}) + \varepsilon \boldsymbol{f}(t), \tag{2.5}$$

where we have added a small perturbation $\varepsilon \boldsymbol{f}(t)$ with $\varepsilon \ll 1$ and $\|\boldsymbol{f}\| = 1$. The dynamics of the phase under perturbation can be determined through

$$\dot{\theta}(t) = \dot{\Theta}(\boldsymbol{q}(t)) = \nabla_{\boldsymbol{q}}\Theta(\boldsymbol{q}) \cdot \dot{\boldsymbol{q}}(t) = \nabla_{\boldsymbol{q}}\Theta(\boldsymbol{q}) \cdot [\boldsymbol{F}(\boldsymbol{q}) + \varepsilon \boldsymbol{f}(t)]. \tag{2.6}$$

We can evaluate $\nabla_{\boldsymbol{q}}\Theta$ along the limit cycle with $\boldsymbol{q}_0$, assuming that the higher-order terms are negligible since the added perturbation is weak. Recalling (2.4), we then arrive at

$$\dot{\theta}(t) = \omega_n + \varepsilon \boldsymbol{Z}(\theta) \cdot \boldsymbol{f}(t), \tag{2.7}$$

https://doi.org/10.1017/jfm.2018.327 Published online by Cambridge University Press

where $\boldsymbol{Z}(\theta) \equiv \nabla_{\boldsymbol{q}}\Theta(\boldsymbol{q})|_{\boldsymbol{q}=\boldsymbol{q}_0}$ is called the phase-sensitivity function. Given the perturbation function, we can determine the influence of the perturbation function on the phase dynamics through (2.7) if $\boldsymbol{Z}(\theta)$ is known.

This phase-sensitivity function can be determined in two ways (Nakao 2016). We can find $\boldsymbol{Z}(\theta)$ by examining the phase response to impulse perturbations (direct method) or by considering the adjoint dynamics (adjoint method; Ermentrout & Terman 2010). In this work, we consider the former impulse-response approach which can be used in both computational and experimental studies. We consider here the influence of a weak impulse perturbation $\boldsymbol{I} = I\delta(t - t_0)h(\boldsymbol{x})\hat{\boldsymbol{e}}_f$ on the state variable $\boldsymbol{q}$, where $\hat{\boldsymbol{e}}_f$ is the unit vector in the forcing direction and $h(\boldsymbol{x})$ describes the spatial profile of the impulse. This impulse can be added to the governing dynamics, such that

$$\dot{\boldsymbol{q}} = \boldsymbol{F}(\boldsymbol{q}) + \boldsymbol{I} \tag{2.8}$$

at some phase θ (at a chosen t_0). With the introduction of this impulse, the phase dynamics becomes affected, causing a shift in the phase along the limit cycle state at steady oscillating conditions.

The phase change at asymptotic state in response to the impulse is known as the phase-response function $g(\theta; I\hat{\boldsymbol{e}}_f)$ and is dependent on the phase at which the impulse is added as well as its location and strength, as illustrated in figure 2(*a*). Given a weak perturbation, the phase-sensitivity function can be evaluated as

$$Z_j(\theta) = \lim_{I\to 0} \frac{g(\theta; I\hat{\boldsymbol{e}}_f)}{I} \approx \frac{g(\theta; I\hat{\boldsymbol{e}}_f)}{I}. \tag{2.9}$$

By introducing the impulse perturbations over a range of θ, the phase-sensitivity function can be determined, as shown in figure 2(*b*). If the phase dynamics of the state variable $\boldsymbol{q}$ is followed by an observable (sensor output), the observable, such as lift in figure 2(*a*), can be used to determine the phase response. This enables experimental efforts with limited measurements to determine the phase-sensitivity function without difficulty.

2.3. *Synchronization of phase dynamics to external oscillation*

With the oscillatory dynamics of fluid flow reduced to its phase dynamics, we can further analyse the condition for which the flow exhibits synchronization to an external periodic perturbation $\boldsymbol{f}(t)$ with a frequency ω_f (and period $T_f = 2\pi/\omega_f$) that is close to ω_n. To facilitate our analysis, we consider the relative phase $\phi(t)$ between the phase $\theta(t)$ of the flow and the phase of the perturbation $\omega_f t$,

$$\phi(t) \equiv \theta(t) - \omega_f t. \tag{2.10}$$

Using (2.7), we find that the time rate of change of the relative phase is

$$\dot{\phi}(t) = \omega_n - \omega_f + \varepsilon \boldsymbol{Z}(\phi(t) + \omega_f t) \cdot \boldsymbol{f}(t) = \varepsilon[\Delta + \boldsymbol{Z}(\phi(t) + \omega_f t) \cdot \boldsymbol{f}(t)], \tag{2.11}$$

where the difference in the natural frequency ω_n and the perturbation frequency ω_f is expressed as $\varepsilon\Delta = \omega_n - \omega_f$, with $\Delta = O(1)$.

By examining the stability characteristics, we can determine when the oscillatory dynamics of the flow can synchronize to external oscillation. That is, when $|\dot{\phi}| \to 0$, the oscillation frequency of the flow converges towards the actuator frequency. At this moment, equation (2.11) describes the dynamics of the phase difference $\phi(t)$ in a

https://doi.org/10.1017/jfm.2018.327 Published online by Cambridge University Press

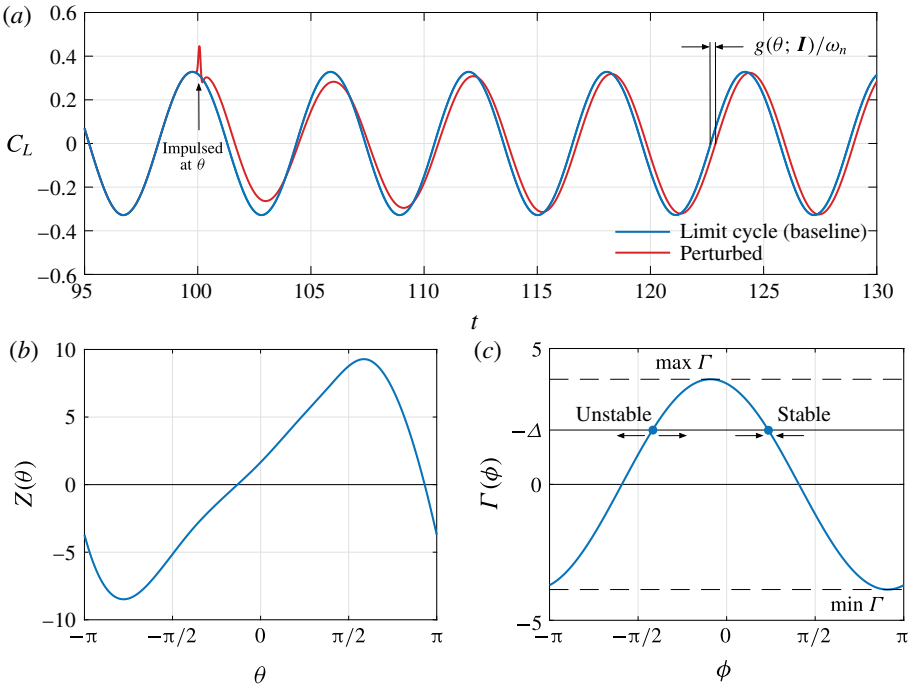


FIGURE 2. (*a*) Determination of the phase-response function $g(\theta; \boldsymbol{I})$ from the impulse input. (*b*) Phase-sensitivity function. (*c*) Phase-coupling function and stability condition for the phase difference ϕ between the system dynamics and the oscillatory actuation. For graphical clarity, $I = 0.025$ is used here. All subsequent phase-reduction analysis uses $I = 0.01$.

non-autonomous manner. To perform a stability analysis, it is desirable to have (2.11) expressed in autonomous form. By realizing that $\phi(t)$ varies slowly compared with $\omega_f t$, we can approximate the right-hand side of (2.11) by its average over a period of actuation (Kuramoto 1984; Ermentrout & Terman 2010) to arrive at

$$\dot{\phi}(t) = \varepsilon[\Delta + \Gamma(\phi)], \tag{2.12}$$

where

$$\Gamma(\phi) = \frac{1}{T_f}\int_t^{t+T_f} \boldsymbol{Z}(\phi + \omega_f \tau)\cdot\boldsymbol{f}(\tau)\,\mathrm{d}\tau = \frac{1}{2\pi}\int_{-\pi}^{\pi} \boldsymbol{Z}(\phi + \psi)\cdot\boldsymbol{f}(\psi/\omega_f)\,\mathrm{d}\psi. \tag{2.13}$$

The function $\Gamma(\phi)$ is 2π-periodic and is known as the phase-coupling function. With (2.12), we now have a one-dimensional autonomous evolution equation for ϕ.

Through inspection of (2.12), we find that the dynamics exhibits stable behaviour if $\min_\phi \Gamma(\phi) < -\Delta < \max_\phi \Gamma(\phi)$, which translates to

$$\varepsilon \min_\phi \Gamma(\phi) < \omega_f - \omega_n < \varepsilon \max_\phi \Gamma(\phi). \tag{2.14}$$

The phase-coupling function $\Gamma(\phi)$ is shown for the example of cylinder flow in figure 2(*c*) with an illustration of the stability condition. The value of the right-hand

https://doi.org/10.1017/jfm.2018.327 Published online by Cambridge University Press

side of (2.12) describes the directions of the solution with respect to the equilibrium points, which are indicated by the arrows in figure 2(*c*). These conditions determine the region of stability over the ω_f–ε space, known as the Arnold tongue (Arnold 1997). This will be shown later in § 3.3 (see figure 5). The decay of the frequency difference between the natural limit cycle and the forcing input constitutes the synchronization of the dynamics (they can have a constant offset in phase under synchronization). Strictly speaking, the above condition for synchronization holds for small forcing input $\varepsilon \ll 1$. While the above analysis assumes that ω_f and ω_n are close to one another for the averaging operation to be a valid approximation, the analysis can be easily extended to consider subharmonic and superharmonic frequencies.

For fluid flows, such synchronization amounts to the so-called lock on. The above result enables us to determine the combination of actuation frequency and amplitude for the flow to synchronize with periodic excitations. As long as we can examine the system response against impulse inputs, the overall formulation can be performed through numerical simulations or experiments, which is attractive for fluid mechanics.

3. Phase-response analysis of an unsteady cylinder wake

3.1. *Model problem*

We apply phase-reduction analysis to examine the synchronization of a circular cylinder wake to periodic forcing. The base periodic flow is taken to be the two-dimensional incompressible flow over a circular cylinder at a diameter-based Reynolds number of $Re \equiv U_\infty d/\nu = 100$, where U_∞, d and ν denote the characteristic free-stream velocity, cylinder diameter and kinematic viscosity of the flow respectively. The dynamics of the flow (2.1) is governed by the non-dimensional incompressible Navier–Stokes equations,

$$\frac{\partial \boldsymbol{u}}{\partial t} + \boldsymbol{u}\cdot\nabla\boldsymbol{u} = -\nabla p + Re^{-1}\nabla^2\boldsymbol{u} + \varepsilon\boldsymbol{f} \quad \text{and} \quad \nabla\cdot\boldsymbol{u} = 0, \tag{3.1a,b}$$

where $\boldsymbol{u}$ is the velocity and p is the pressure. In this equation, the forcing (actuation) input $\varepsilon\boldsymbol{f}$ is taken to be a localized force (momentum injection)

$$\varepsilon\boldsymbol{f} = \delta(\boldsymbol{x}-\boldsymbol{x}_f)\eta(t)\hat{\boldsymbol{e}}_f \tag{3.2}$$

having a magnitude of $\varepsilon \ll 1$, position of $\boldsymbol{x}_f$ and forcing direction specified by a unit vector $\hat{\boldsymbol{e}}_f$. The Dirac delta in space is approximated using the three-cell discrete delta function (Roma, Peskin & Berger 1999). The overall set-ups of the forcing input for the two cases considered below are illustrated in figure 3.

The function $\eta(t)$ specifies the temporal form of the forcing input as

$$\eta(t) = \begin{cases} I\delta(t) \approx \dfrac{I}{\sqrt{2\pi}\sigma}\exp\left[-\dfrac{1}{2}\left(\dfrac{t-t_0}{\sigma}\right)^2\right] & \text{for impulse perturbation,} \\ \dfrac{\varepsilon}{2}[1+\sin(\omega_f t+\psi)] & \text{for periodic perturbation.} \end{cases} \tag{3.3}$$

The impulse perturbation, approximated as a narrow Gaussian in time (with $\sigma = 0.005$), is introduced to the flow to determine the phase-response, phase-sensitivity and phase-coupling functions. The sinusoidal forcing function is chosen to examine the lock-on behaviour of the flow to periodic flow control input. While the impulse

https://doi.org/10.1017/jfm.2018.327 Published online by Cambridge University Press

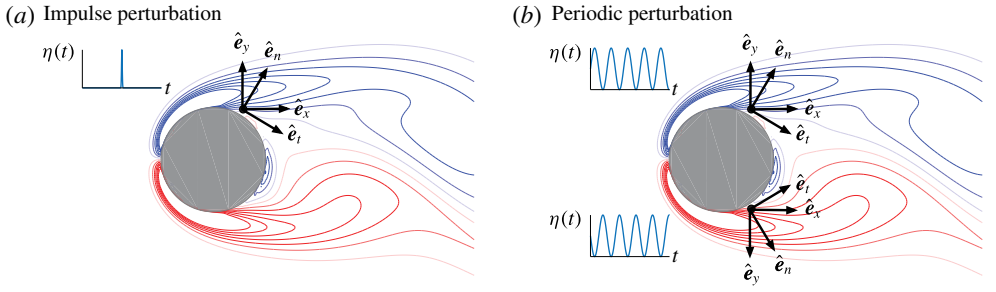


FIGURE 3. The cylinder flow forcing set-up to analyse (*a*) the impulse response with a top actuator only and (*b*) the effect of periodic forcing with top and bottom actuators. The selected forcing directions are the x direction (x), the y direction (y), tangential (t) and normal (n).

	C_L	C_D	St
Present	± 0.328	1.345 ± 0.009	0.165
Liu, Zheng & Sung (1998)	± 0.339	1.35 ± 0.012	0.165
Linnick & Fasel (2005)	± 0.337	1.34 ± 0.009	0.165
Canuto & Taira (2015)	± 0.329	1.34 ± 0.0091	0.167

TABLE 1. Comparison of lift, drag and Strouhal number (St) for circular cylinder flow at $Re = 100$.

perturbation is introduced only at the top separation point (58.4° from the aft separation point, positioned $3\Delta x$ away from the surface), we add the sinusoidal forcing input at the top and bottom separation points with a phase difference of ϕ (top $\psi = 0$ and bottom $\psi = \pi$). The actuation is introduced near the separation points to effectively modify the wake dynamics. However, the perturbations can be added to any locations in the flow field for this analysis. The forcing amplitudes are chosen such that $I = 0.01$ and $\varepsilon \in [0, 0.1]$. The corresponding steady and oscillatory momentum coefficients for the periodically forced cases are less than 0.02 and 0.007 respectively for $\varepsilon \leqslant 0.1$ (Munday & Taira 2013).

3.2. *Computational set-up*

The immersed boundary projection method simulates the unsteady flow on a Cartesian grid with the cylinder represented through the boundary forcing (Taira & Colonius 2007). For the present study, the fast version of the immersed boundary projection method is chosen (Colonius & Taira 2008), with the computational domain extending over $(x/d, y/d) \in [-31, 33] \times [-32, 32]$. The grid near the cylinder has $\Delta x_{min}/d = \Delta y_{min}/d = 0.02$ and the time step is chosen to meet $U_\infty \Delta t/\Delta x_{min} = 0.5$. The computational algorithm and set-up have been validated extensively in past studies, including a similar study on control of cylinder flow (Munday & Taira 2013). The present study captures the baseline flow accurately and agrees with findings from three independent numerical codes, as summarized in table 1.

https://doi.org/10.1017/jfm.2018.327 Published online by Cambridge University Press

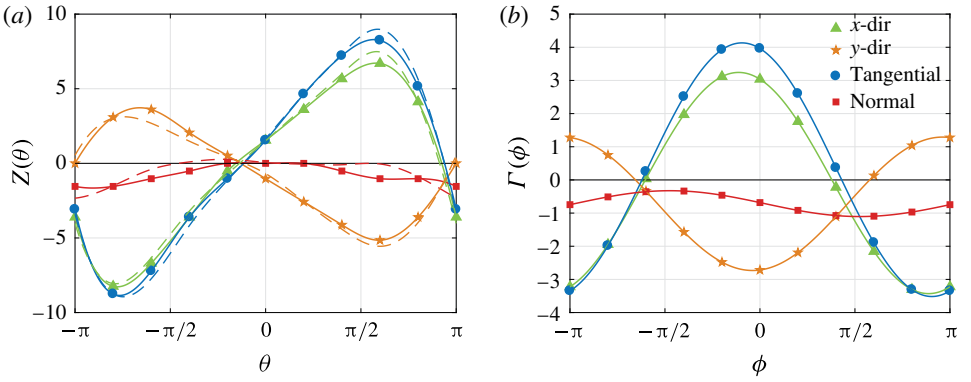


FIGURE 4. (*a*) The phase-sensitivity function $Z(\theta)$ and (*b*) phase-coupling function $\Gamma(\phi)$ for the cylinder wake and periodic forcing input. The dashed lines for the phase-sensitivity function show approximations from complementary bases. Symbols represent where actual simulations were performed.

3.3. *Analysis of the cylinder wake*

In this section, we determine the phase-response, phase-sensitivity and phase-coupling functions to characterize the cylinder flow dynamics in terms of phase on the $\dot{C}_L$–C_L space. Once these functions are determined, we can find the conditions for synchronization of the cylinder wake to periodic perturbations.

We first characterize the phase response of the cylinder wake to weak impulse perturbations added near the top separation point. By evaluating the change in phase, we can determine the phase-response function $g(\theta; I\hat{\boldsymbol{e}}_f)$. The magnitude of the impulse is set to $I = 0.01$, which is small in magnitude compared with the force on the cylinder. Here, we consider adding the impulse in four different directions (x, y, surface-tangential and surface-normal directions) from the top separation point, as illustrated in figure 3. These directions are chosen to form two pairs of orthogonal directions, such that they can serve as bases for subsequent analyses.

Based on the impulse responses, we can compile in figure 4(*a*) the phase-sensitivity function $Z(\theta)$ evaluated with (2.9) over the phase space for the four directions, shown by the solid lines. Symbols represent where actual simulations were performed; 10 simulations were performed for each direction. Impulse added in the tangential and x directions leads to phase advancement. The tangential forcing exhibits the largest phase sensitivity among the four directions examined. Forcing in the y direction causes phase delay, and normal forcing does not result in much of a phase change. We also show with dashed lines in figure 4(*a*) the phase-sensitivity functions found by rotating the coordinate systems. That is, the x and y components are evaluated based on the tangential and normal components, and *vice versa*. The close agreement between the solid and dashed lines suggests that the chosen impulse magnitude is adequately small for the linear approximations made in (2.7) and (2.9) to hold. Hence, it suffices to perform the impulse-response analysis in two independent forcing directions to map out the phase-sensitivity function over the phase space. In this example, the phase-sensitivity function quantifies the sensitivity of the shear layer dynamics aft of the separation point (as well as the overall wake vortex dynamics) to the added impulse perturbation.

With the phase-sensitivity function $Z(\theta)$ available, the phase-coupling function $\Gamma(\phi)$ can be found through (2.13). For the present periodic forcing case, we need

https://doi.org/10.1017/jfm.2018.327 Published online by Cambridge University Press

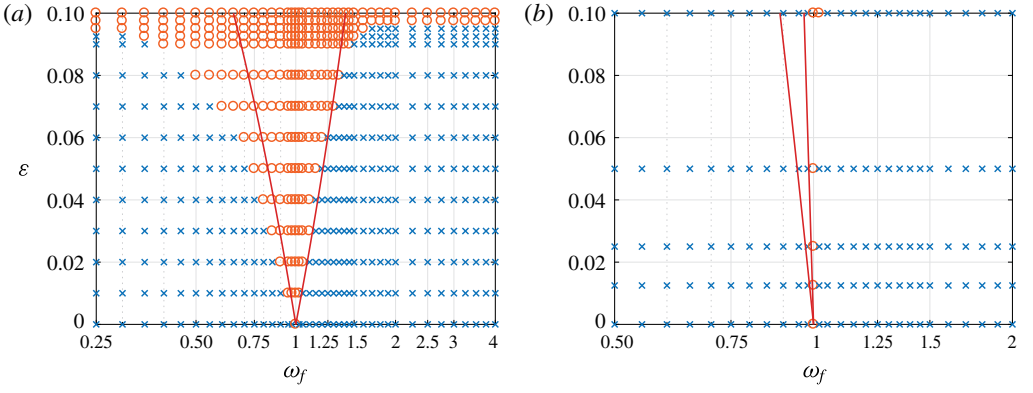


FIGURE 5. Synchronization of the cylinder wake to periodic actuation for (*a*) tangential and (*b*) normal forcing inputs. Synchronized and unsynchronized cases from DNS (Munday & Taira 2013) are shown by ○ and × respectively. The criteria for synchronization (2.14) correspond to the region bounded by the red lines.

to sum the influences of the top and bottom actuators, which essentially doubles the magnitude of $\eta(t)$ in the computation of $\Gamma(\phi)$. The phase-coupling functions for the four representative directions are shown in figure 4(*b*). As expected, large variations in $\Gamma(\phi)$ over the relative phase ϕ are given by the periodic perturbations in the tangential and x directions. Forcing in the y direction has opposing effects with reduced variation. Normal forcing seems to be the least influential among these four directions. It is interesting to note that $Z(\theta)$ has a zero average over θ for the tangential forcing case, which removes the influence of non-zero mean of the forcing input.

It should be recalled that greater variations in the phase-coupling function widen the regions for achieving synchronization of the wake dynamics to actuation fluctuation, as stated in condition (2.14). For example, tangential and normal direction forcing yield $(\min \Gamma, \max \Gamma) = (-3.52, 4.13)$ and $(-1.10, 0.33)$ respectively. We can take these minimum and maximum values for the synchronization condition and compare them with the results from direct numerical simulations (DNS) (Munday & Taira 2013), as summarized in figure 5. In the work of Munday & Taira (2013), the cylinder wake is considered to be synchronized (locked on) to the actuation frequency when the lift power spectrum exhibits a single peak at the actuation frequency.

For the tangential forcing cases shown in figure 5(*a*), the condition for synchronization from the phase-response analysis agrees well with the full nonlinear wake simulations capturing the region of the Arnold tongue, especially for low forcing amplitude ε until nonlinear effects become apparent at higher $\varepsilon \gtrsim 0.07$. As mentioned earlier, the phase-sensitivity function for tangential forcing removes the influence of the non-zero forcing input for synchronization. In fact, the region of lock on is not altered much for a zero-mean forcing case, as presented in the DNS findings (Munday & Taira 2013). For $\varepsilon \gtrsim 0.097$, the wake becomes synchronized to the oscillatory forcing for all considered actuation frequencies, which is beyond the validity of the present phase-reduction analysis.

For the normal forcing case, we observe that the Arnold tongue is much narrower than that of the tangential forcing case, as is evident from figure 5(*b*). The phase-reduction analysis predicts the narrow width of the synchronization region well, but

https://doi.org/10.1017/jfm.2018.327 Published online by Cambridge University Press

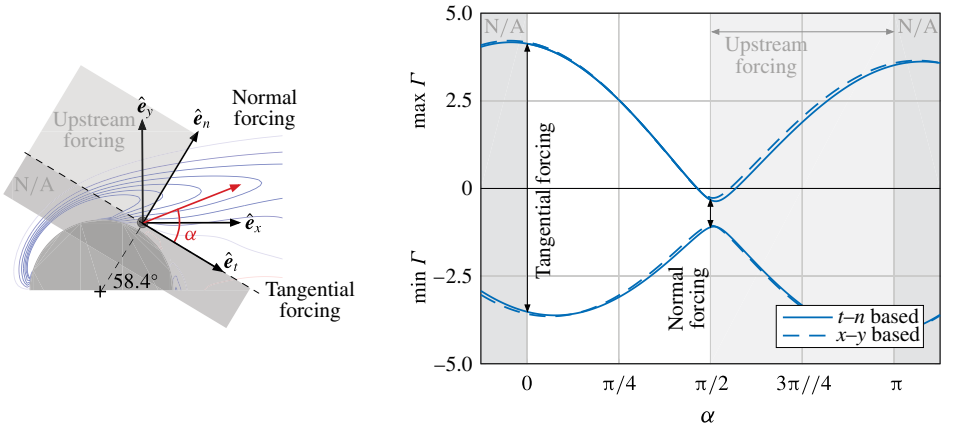


FIGURE 6. Minimum and maximum values of the phase-coupling function Γ over the forcing angle α measured from the tangential direction. Extrema based on the x and y directions as well as the tangential and normal directions are shown. The forcing directions and angle α are depicted on the left.

slightly biases the tongue towards lower frequency, which becomes obvious for higher forcing amplitudes. This deviating trend from normal forcing is probably caused by the inaccuracy in the evaluation of the small-amplitude phase-sensitivity function as well as by the nonlinear effects.

The identification of the Arnold tongue from the phase-response analysis is attractive since we only require a limited number of simulations to determine the phase-response function over the phase $\theta \in [-\pi, \pi]$. Instead of having to perform a large number of full DNS (or experiments) as a parametric study to locate the Arnold tongue, we can analytically determine the boundary of synchronization from the phase-coupling function. Moreover, for two-dimensional flow, we can consider two independent forcing directions to determine the impulse response for any forcing direction, as depicted in figure 6. By constructing the phase-sensitivity function over the forcing direction α based on the tangential and normal components or the x and y components, we can determine the minimum and maximum values of Γ as a function of α, as shown in figure 6. In this figure, we shade out the directions that would be directed below the tangential direction (into the body) as well as the upstream direction (acting against the free stream). Restricting our interest to downstream forcing in the range $\alpha \in [0, \pi/2]$, we find that synchronization can be achieved for the widest range of ω_f with tangential forcing ($\alpha \approx 2°$). On the other hand, normal forcing would be the most difficult to achieve synchronization with, due to its narrowest bound over α. We emphasize that the bounds for synchronization have been determined with only a limited number of simulations and do not require an extensive parameter sweep, which significantly reduces the need for computational (and experimental) resources.

While synchronization in this particular example leads to drag increase for the majority of the synchronized cases, phase-response analysis shows tremendous potential to identify the condition of lock on for a range of fluid flow problems. In this example, we know from our previous work (Munday & Taira 2013) that the addition of non-zero mean in tangential forcing can achieve drag reduction and with minimal effect of altering the lock-on region. In fact, the zero-mean case also

https://doi.org/10.1017/jfm.2018.327 Published online by Cambridge University Press

shows good agreement with the predicted condition for synchronization. There are other cylinder flow examples that can achieve drag reduction, for example the case of synchronizing the wake to the sinusoidal rotation of the cylinder (Tokumaru & Dimotakis 1991).

For the presently considered periodically forced cylinder wake, we do not observe subharmonic or superharmonic synchronizations from DNS. There are of course other fluid flows that exhibit such behaviour. Phase-response analysis can be extended to determine the condition for synchronization near harmonic frequencies.

4. Conclusion

We have applied phase-reduction analysis to periodic fluid flows to study the phase dynamics and synchronization properties. This was achieved by capturing the oscillatory physics through its scalar phase dynamics. With such a formulation, we were able to determine the phase response to impulse perturbations, which formed the basis to evaluate the influence of external perturbations on the oscillatory flow dynamics. These insights reveal the Arnold tongue over which the flow can exhibit synchronization to periodic excitation. As an example, we have considered the unsteady wake dynamics behind a circular cylinder and characterized the synchronization properties for momentum-based forcing. Comparison with DNS showed close agreement with the phase-based analysis. The present study also confirmed that the tangential forcing direction is the optimal direction to achieve lock on for the widest range of actuation frequency. This phase-based analysis can be performed in numerical simulations and experiments, holding promising potential to uncover synchronization properties for a large class of problems, including wake dynamics, flow control, vortex-induced vibration, fluid–structure interaction and reacting flows, without the need for extensive parametric sweeps.

Acknowledgements

K.T. gratefully acknowledges the support from the US Air Force Office of Scientific Research (grant FA9550-18-1-0040; Program Manager Dr D. R. Smith) and the US Army Research Office (grant W911NF-17-1-0118; Program Manager Dr M. J. Munson). H.N. acknowledges financial support from the Japan Society for the Promotion of Science KAKENHI grants JP16H01538, JP16K13847 and JP17H03279.

References

ARNOLD, V. I. 1997 *Mathematical Methods of Classical Mechanics*. Springer.

BUCK, J. 1988 Synchronous rhythmic flashing of fireflies. II. *Q. Rev. Biol.* **63** (3), 265–289.

CANUTO, D. & TAIRA, K. 2015 Two-dimensional compressible viscous flow around a circular cylinder. *J. Fluid Mech.* **785**, 349–371.

COLONIUS, T. & TAIRA, K. 2008 A fast immersed boundary method using a nullspace approach and multi-domain far-field boundary conditions. *Comput. Meth. Appl. Mech. Engng* **197**, 2131–2146.

ERMENTROUT, G. B. & TERMAN, D. H. 2010 *Mathematical Foundations of Neuroscience*. Springer.

GUCKENHEIMER, J. 1975 Isochrons and phaseless sets. *J. Math. Biol.* **1** (3), 259–273.

KAWAMURA, Y. & NAKAO, H. 2013 Collective phase description of oscillatory convection. *Chaos* **23**, 043129.

KAWAMURA, Y. & NAKAO, H. 2015 Phase description of oscillatory convection with a spatially translational mode. *Physica* D **295–296**, 11–29.

KURAMOTO, Y. 1984 *Chemical Oscillations, Waves, and Turbulence*. Springer.

https://doi.org/10.1017/jfm.2018.327 Published online by Cambridge University Press

LINNICK, M. N. & FASEL, H. F. 2005 A high-order immersed interface method for simulating unsteady incompressible flows on irregular domains. *J. Comput. Phys.* **204**, 157–192.

LIU, C., ZHENG, X. & SUNG, C. H. 1998 Preconditioned multigrid methods for unsteady incompressible flows. *J. Comput. Phys.* **139**, 35–57.

MAUROY, A. & MEZIĆ, I. 2012 On the use of Fourier averages to compute the global isochrons of (quasi)periodic dynamics. *Chaos* **22**, 033112.

MUNDAY, P. M. & TAIRA, K. 2013 On the lock-on of vortex shedding to oscillatory actuation around a circular cylinder. *Phys. Fluids* **25**, 013601.

NAKAO, H. 2016 Phase reduction approach to synchronisation of nonlinear oscillators. *Contemp. Phys.* **57** (2), 188–214.

PIKOVSKY, A., ROSENBLUM, M. & KURTHS, J. 2001 *Synchronization: A Universal Concept in Nonlinear Sciences*. Cambridge University Press.

ROMA, A. M., PESKIN, C. S. & BERGER, M. J. 1999 An adaptive version of the immersed boundary method. *J. Comput. Phys.* **153**, 509–534.

STROGATZ, S. H. 2000 From Kuramoto to Crawford: exploring the onset of synchronization in populations of coupled oscillators. *Physica* D **143**, 1–20.

TAIRA, K. & COLONIUS, T. 2007 The immersed boundary method: a projection approach. *J. Comput. Phys.* **225**, 2118–2137.

TOKUMARU, P. T. & DIMOTAKIS, P. E. 1991 Rotary oscillation control of a cylinder wake. *J. Fluid Mech.* **224**, 77–90.

WINFREE, A. T. 1967 Biological rhythms and the behavior of populations of coupled oscillators. *J. Theor. Biol.* **16** (1), 15–42.

YAMAGUCHI, Y., SUZUKI, T., MIZORO, Y., KORI, H., OKADA, K., CHEN, Y., FUSTIN, J.-M., YAMAZAKI, F., MIZUGUCHI, N., ZHANG, J. *et al.* 2013 Mice genetically deficient in vasopressin V1a and V1b receptors are resistant to jet lag. *Science* **342**, 85–90.

https://doi.org/10.1017/jfm.2018.327 Published online by Cambridge University Press